ARTICLE

Supporting Information

UV-Robust and Efficient Perovskite Solar Cells Enabled by Interfacial Photocatalysis Suppression and Defects Passivation

Jingwei Zhu,[a] Xumeng Hu,[a] Zhuoyan Liu,[a] Minghuang Guo,[a] Ying Zhang, [a] Yafeng Li,[*a] Junming Li,[a,c] and Mingdeng Wei[*a,b.]

[a] *Fujian Key Laboratory of Electrochemical Energy Storage Materials, Fuzhou University Fuzhou, Fujian 350002, China*
[b] *State Key Laboratory of Photocatalysis on Energy and Environment, College of Chemistry, Fuzhou University, China*
[c] *Beijing Key Laboratory for Sensors, Beijing Information Science & Technology University, Beijing 100192, China*
**E-mail: liyf@fzu.edu.cn; wei-mingdeng@fzu.edu.cn*

Materials and Methods

Materials

PbI_2 (>99.9985%) was obtained from Alfa Aesar. $PbBr_2$, FAI, MAI, CsI and 2,2',7,7'-tetrakis-(N,N-di-4-methoxyphenylamino)-9,9'-spirobifluorene (spiro-OMeTAD) were purchased from Xi'an Polymer Light Technology Corp. titanium diisopropoxide bis(acetylacetonate), 1-Butano, N, N-dimethylformamide (DMF), dimethyl sulfoxide (DMSO), isopropanol (IPA), chlorobenzene (CB), acetonitrile, bis(trifluoromethane) sulfonimide lithium salt (LiTFSI), 4-tert-bultypyridine were acquired from Sigma-Aldrich. FTO substrates were customized from SuZhou ShangYang Solar Technology. 4,4'-Oxybisbenzoic Acid (OBBA) was purchased from Adamas Reagent, Ltd. All chemicals were used as received without further purification.

Characterization

FTIR results were obtained by Nicolet Is50 (Thermo Fisher) at 400-4000 cm^{-1}. XPS results were obtained from Thermo ESCALAB 250Xi. The X-ray powder diffraction (XRD) measurement was conducted by Rigaku Ultima IV with Cu Kα radiation (1.5418 Å). The UV-Vis transmission spectra were tested with Shimadzu UV-2450. The morphology of perovskite films were observed by scanning electron microscope (SEM) (FESEM, Hitachi S4800) and atomic force microscopy (AFM) (SPA-300, Bruker). Time-resolved photoluminescence spectroscopy (TRPL) were measured by Edinburgh FLS 980 instrument. Photoluminescence (PL) and PL intensity mapping was obtained by a confocal Raman spectrometer (LabRAM HR Evolution, Horiba scientific), the simple but representative $MAPbI_3$ perovskite was adopted in the Raman test. The devices were tested by a Xe lamp with an AM 1.5 filter (100 $mW \cdot cm^{-2}$) (Peccell) covered by a mask (active area of 0.12 cm^2) and recorded by Keithley 2400 with a scan rate of 30 $mV \cdot s^{-1}$. PEC-S20 (Peccell) was used to measure the Incident photon-to-electron conversion efficiency (IPCE) spectrum. An electrochemical workstation (IM6, Zahner) was used to record the electrochemical impedance spectroscopy (EIS) spectrum, dark *J-V* and dark *I-V* curves. The UV aging test in this work were conducted by putting the unencapsulated devices in a nitrogen-filled glovebox and exposed to a UV lamp (275 nm, 10 mW cm^{-2} or 365 nm, 600 mW cm^{-2}) from the TiO_2 ETL side at room temperature. As for the HPIC measurement, the spin coating speed was 2000 rpm, in order to obtain thicker perovskite films, 5 samples for each group were placed in a quartz reaction tube which were sealed in a nitrogen glove box to increase the production of methylamine gas, after UV irradiation for different times, the gas in the reaction tubes was extracted and injected into the sulfuric acid absorption solution (0.01 mol/L) for testing by HICP. The standard methylamine solution was prepared at 20 ppm. In spectroscopic ellipsometry test

(Horoba UVISEL PLUS), the concentration of OBBA was selected as 0.02 mg mL^{-1}, to ensure the accuracy of the SE measurement, a flat FTO substrate was used, the OBBA layer was prepared by dropping the same volume of DMF as the precursor solution onto OBBA, followed by spin-coating and annealing.

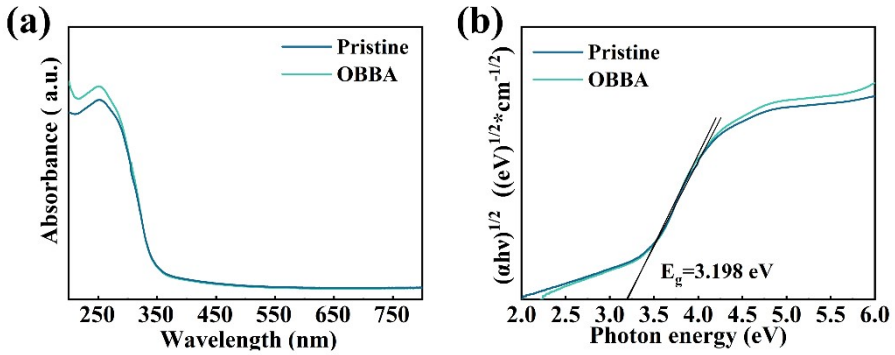

Figure S1 the UV-vis absorption spectra and corresponding Tauc plots of each TiO_2.

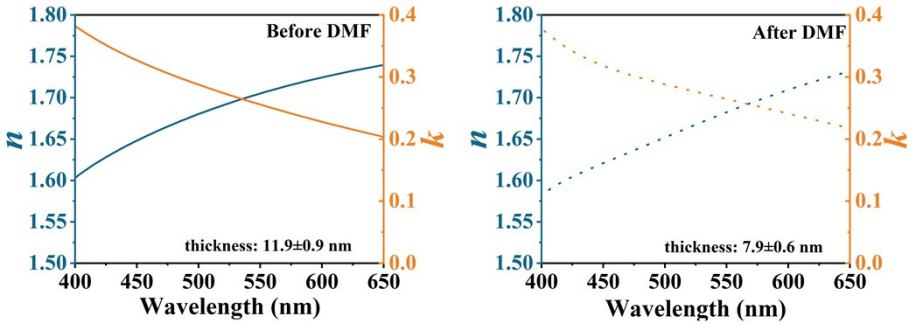

Figure S2 The refractive index (n) and extinction coefficient (k) of OBBA layer measured by spectroscopic ellipsometry.

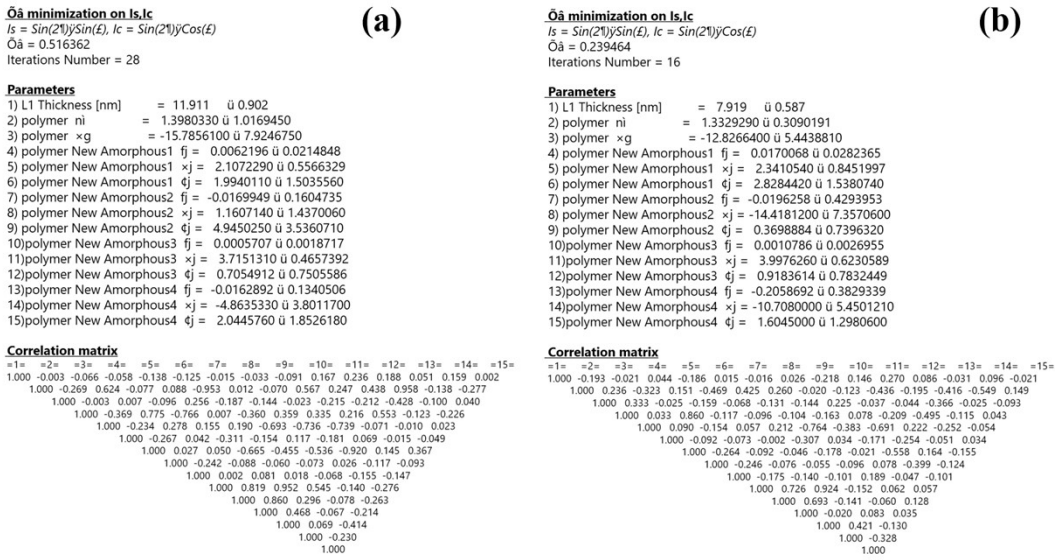

Figure S3 Corresponding fitting parameters and results of OBBA layer in spectroscopic ellipsometry, (a) before spin coating and (b) after spin coating.

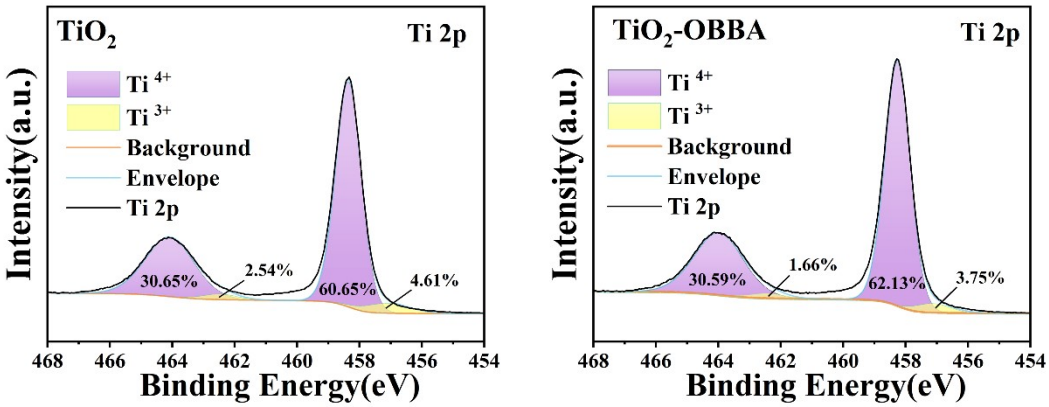

Figure S4. Detailed Ti 2p spectra with area ratio of the (**a**) pristine TiO_2 and (**b**) OBBA-modified TiO_2.

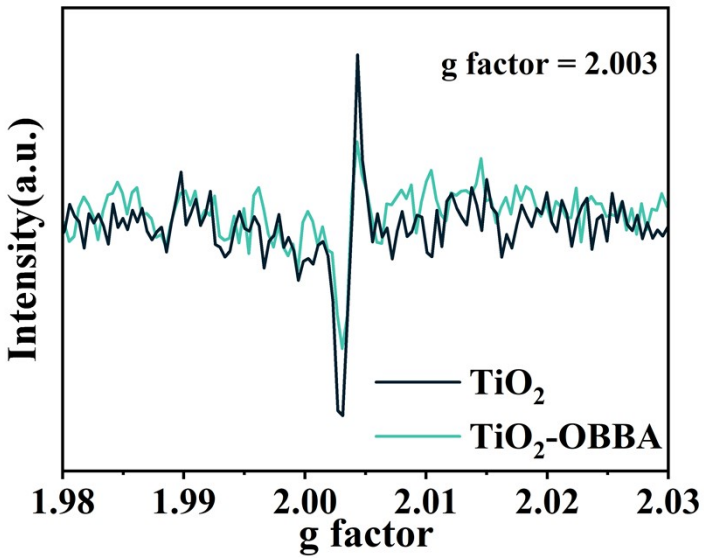

Figure S5. EPR spectra of pristine and TiO_2-OBBA layer.

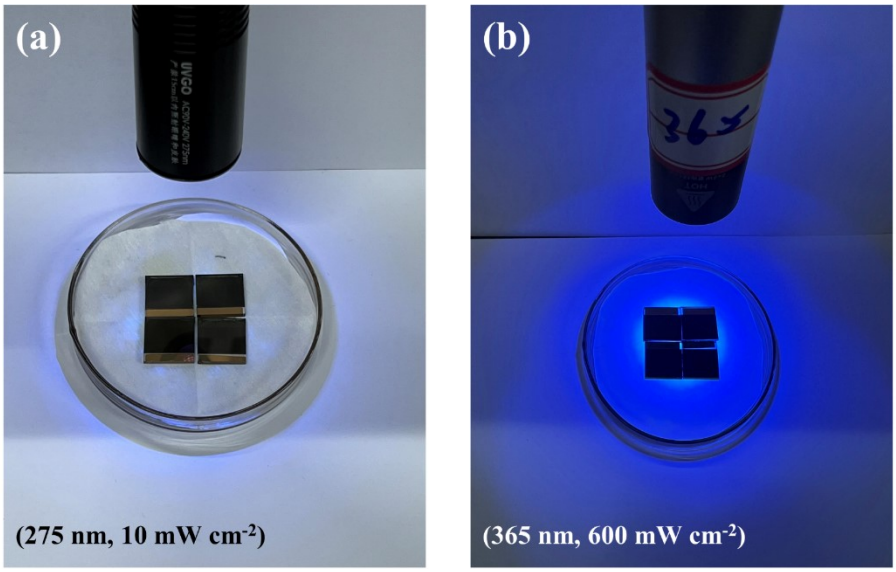

Figure S6. Photograph of the devices under different UV lambs, (a) 275 nm, 10 mW cm^{-2}, and (b) 365 nm, 600 mW cm^{-2}.

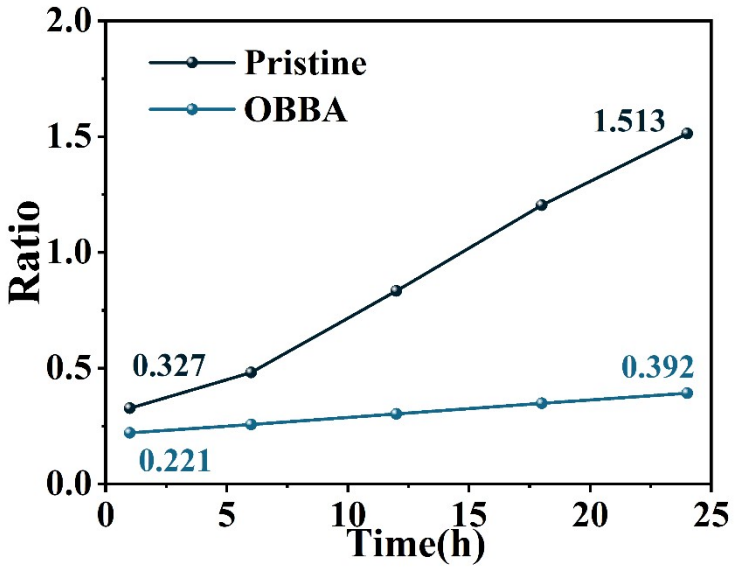

Figure S7. The ratio of peak intensity for PbI_2 and perovskite(001) of the perovskite film based on pristine and OBBA-modified TiO_2.

Figure S8. Photo of the quartz reaction tube for collecting methylamine gas, 5 PSCs were irradiated simultaneously to increase the production of methylamine gas.

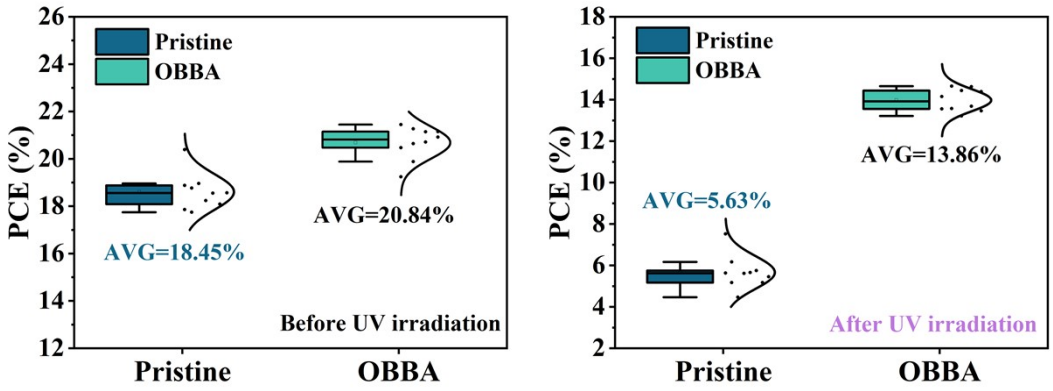

Figure S9 The PCE statistics of the pristine and OBBA PSCs before and after UV illumination.

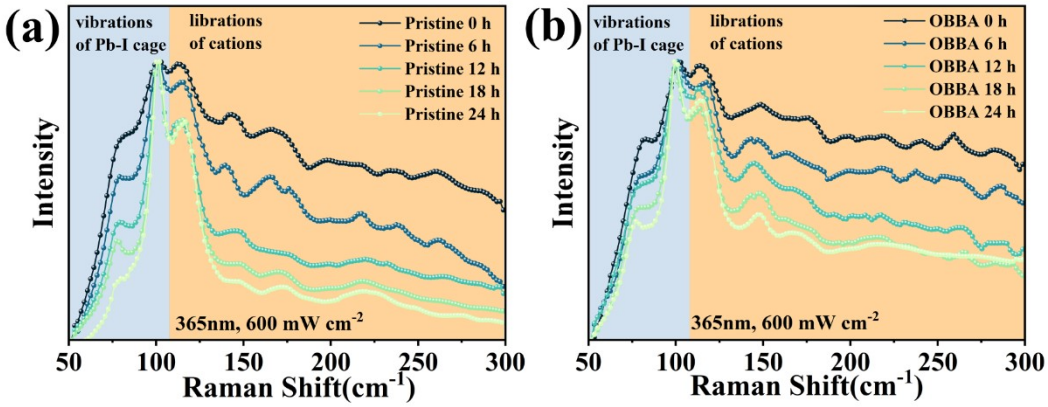

Figure S10. Raman spectra of (a) the pristine and (b) the OBBA-modified device under continuous UV irradiation (365 nm, 600 mW cm^{-2}).

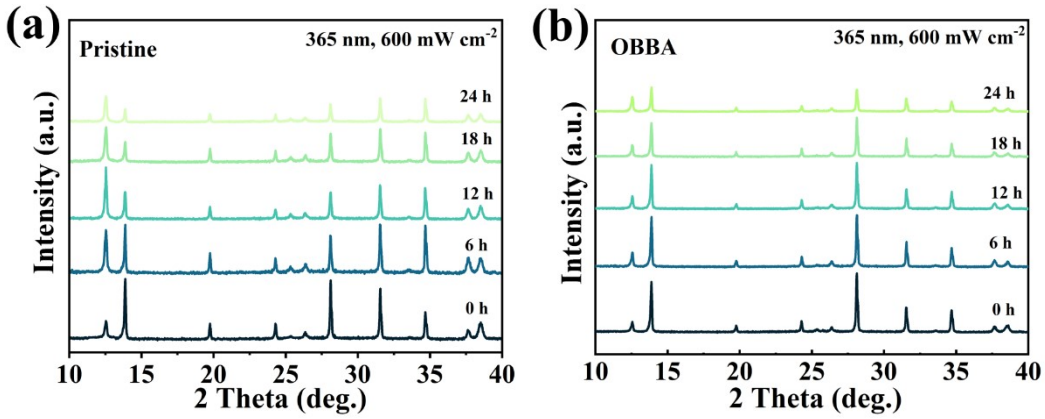

Figure S11. XRD patterns of (c) the pristine and (d) the OBBA-modified device under continuous UV irradiation (365 nm, 600 mW cm^{-2}).

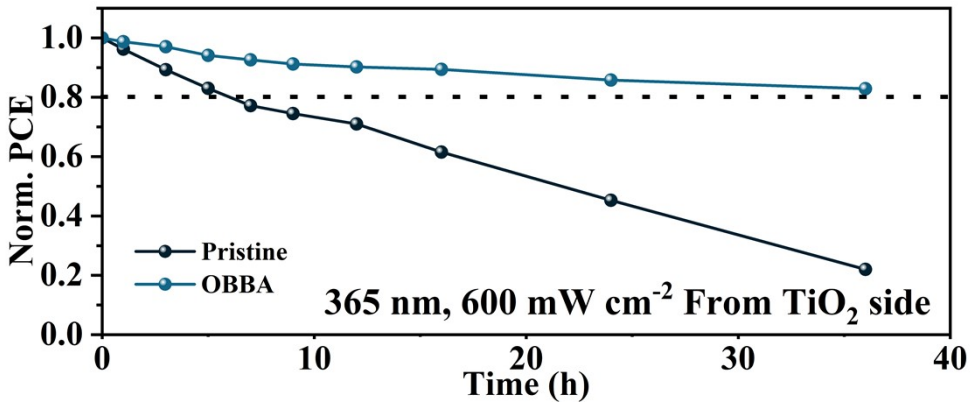

Figure S12. PCE decay of the pristine and the OBBA-modified device under continuous UV radiation(365 nm, 600 mW cm^{-2}).

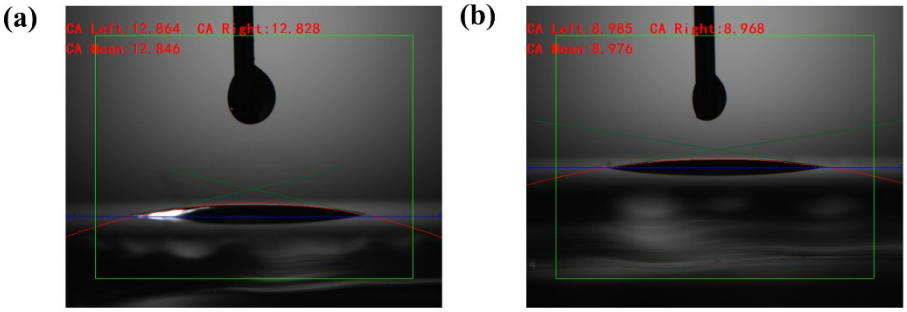

Figure S13. Contact angle of TiO_2 layer (a) without and (b) with OBBA modification.

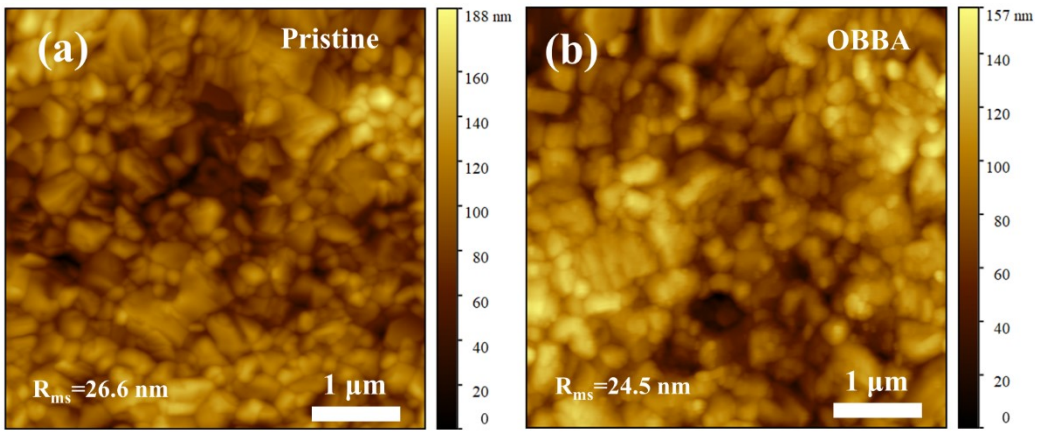

Figure S14. AFM images of the perovskite layer based on (a) pristine and (b) OBBA-modified TiO_2 layer.

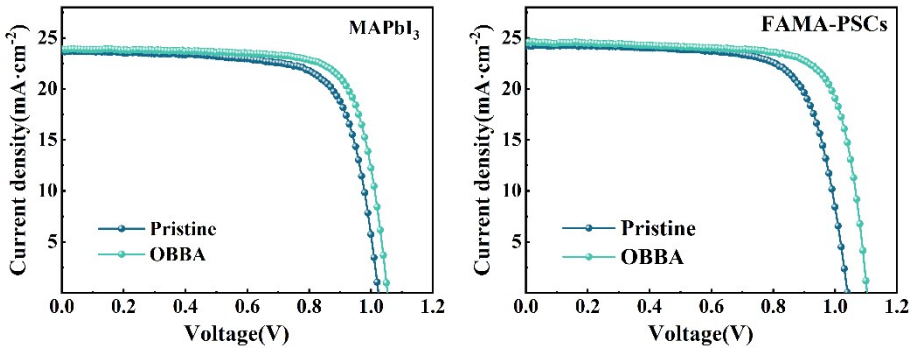

Figure S15. Photovoltaic performance of $MAPbI_3$ and $FAMAPbIBr_3$-based PSCs.

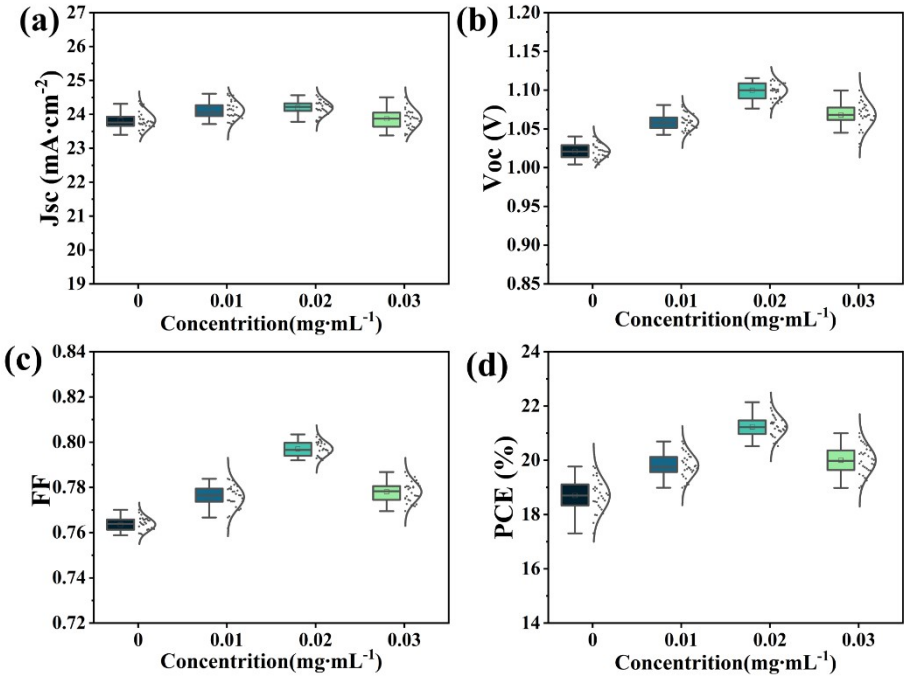

Figure S16. Statistical distributions of photovoltaic parameters for (a) J_{SC}, (b) V_{OC}, (c) FF, and (d) PCE, obtained by *J*−*V* measurements of PSCs based on different concentrations (0, 0.01, 0.02, 0.03 mg mL^{-1}) of OBBA modification, fitted with a Gaussian distribution.

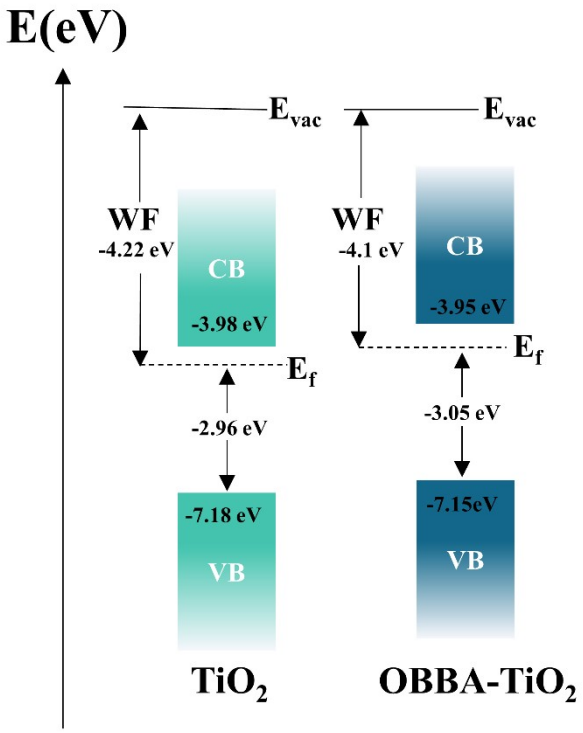

Figure S17. Work function and Fermi level of the PSCs based on (a) pristine and (b) OBBA-modified TiO_2.

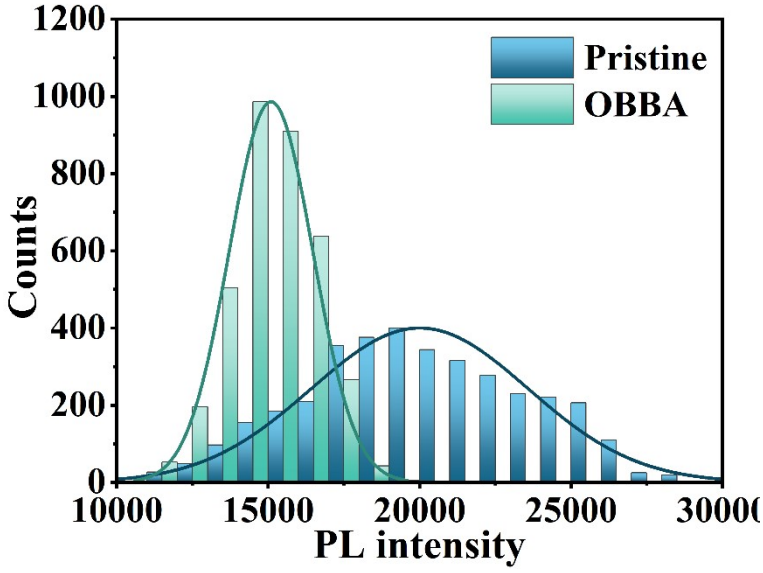

Figure S18. The statistical of the PL intensity for the pristine and OBBA-modified sample obtained from the PL intensity mapping images.

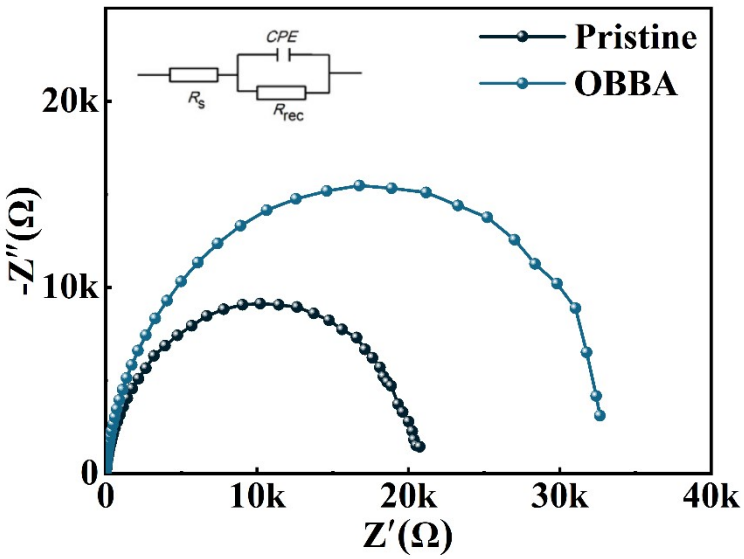

Figure S19. Nyquist plots of the pristine and OBBA-modified PSCs under dark condition.

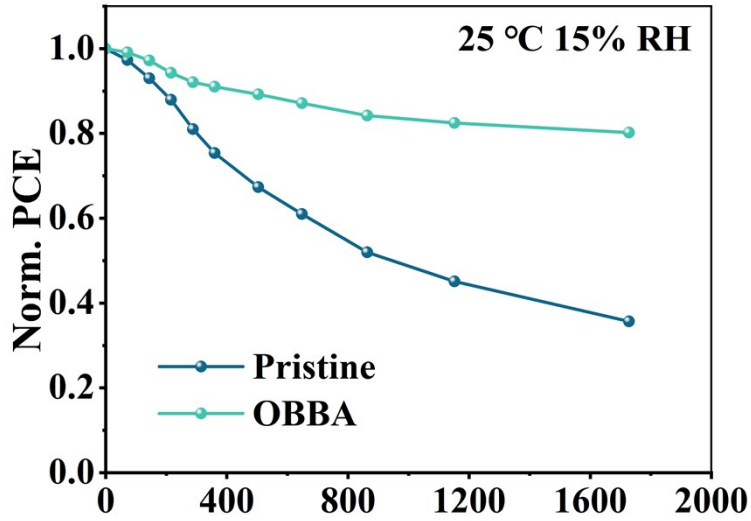

Figure S20. PCE decay of the pristine and the OBBA-modified device under air condition (25℃, 15%RH)

Table S1 Photovoltaic parameters and reverse and forward scans of the MA-PSCs and FAMA-PSCs with/wo OBBA modification.

	J_{sc}/mA·cm^{-2}	V_{oc}/V	FF/%	PCE/%
MA-PSC Pristine	23.65	1.024	72.81	17.63
MA-PSCs OBBA	23.88	1.054	75.89	19.10
FAMA-PSC Pristine	24.20	1.041	72.87	18.35
FAMA-PSC OBBA	24.53	1.103	76.35	20.67

Table S2 Photovoltaic parameters and reverse and forward scans of the PSCs with/wo OBBA modification.

	J_{SC}/mA·cm^{-2}	V_{OC}/V	FF/%	PCE/%	HI (%)
OBBA Reverse	24.83	1.099	78.49	21.42	9.96
OBBA Forward	24.74	1.083	72.24	19.35	
Pristine Reverse	24.45	1.026	75.84	19.03	24.89
Pristine Forward	24.40	1.005	58.28	14.29	

Table S3 Relative data for UPS measurement based on the PSCs with/wo OBBA modification.

Sample	$E_{\text{cut-off}}$	$E_{\text{on-set}}$	W_F	E_{CBM}	E_{VBM}
Pristine	17.00	2.96	-4.22	-3.98	-7.18
OBBA	17.12	3.05	-4.1	-9.95	-7.15

Table S4 Steady-state PL quenching of perovskite film on the indicated substrates.

Substrate	PL quenching (%)
Glass	N/A
TiO_2	90.55
TiO_2-OBBA	94.49

Table S5 Fitted data for time-resolved PL lifetimes of perovskite films on the indicated ETLs from the biexponential decay mode.

Sample	A_1%	τ_1/ns	A_2%	τ_2/ns	τ_{avg}[c]/ns
Pristine	14.74	9.12	85.26	366.23	364.70
OBBA	2.96	4.51	97.04	242.88	242.75

$$\tau_{ave} = \sum A_i \tau_i^2 / \sum A_i \tau_i$$

Table S6 EIS parameters of the PSCs based on different concentrations of OBBA modification under dark condition.

Sample	R_s/Ω	R_{ct}/Ω	R_{rec}/Ω
Pristine	11.62	47.57	20743
OBBA	10.16	36.06	33578

Table S7 Comparison of several representative UV-robust PSCs under different UV radiation conditions.

Ref.	Device Structure	Condition	Time (h)	PCE after UV
Our work	FTO/c-TiO_2 /m-TiO_2/OBBA/perovskite/Spiro-OMeTAD/Au	275 nm, 10 mW cm^{-2}	72	70
Our work	FTO/c-TiO_2/m-TiO_2/OBBA/perovskite/Spiro-OMeTAD/Au	365 nm, 600 mW cm^{-2}	36	83
1	FTO/Mg_xZnO_{1-x}/perovskite/PTAA/Au	365 nm, 35 mW cm^{-2}	8h	76%
2	ITO/SnO_2/ClMPI/MAPbI3/Spiro-OMeTAD/Au	365 nm, 100 mW cm^{-2}	500h	82%
3	FTO/Eu-TiO_2/$(Cs_{0.05}FA_{0.80}MA_{0.15})Pb(I_{0.85}Br_{0.15})_3$/Spiro-OMeTAD/Au	365 nm, 5 mW cm^{-2}	500h	75%
4	FTO/SnO_2/CsFAMA-lycopene/Spiro-OMeATD/Ag	365nm, 600 mW cm^{-2}	8h	84%
5	FTO/SnO_2-2-hydroxy-4-methoxy-5-sulfonate-benzophenone/perovskite/Spiro-OMeTAD/Au	285 nm, 1.63 mW cm^{-2}	200h	95%
6	ITO/SnO_2/Perovskite/sunscreen-perovskite/Spiro-OMeTAD/Au	285 nm, 1.35 mW cm^{-2}	24h	80%
6	ITO/SnO_2/Perovskite/sunscreen-perovskite/Spiro-OMeTAD/Au	365nm, 600 mW cm^{-2}	6h	80%
7	FTO/c-TiO_2 /TiO_2(CsBr)/perovskite/ Spiro-OMeTAD/Au	365nm, 523 mW cm^{-2}	20min	70%
8	FTO/c-TiO_2 /TiO_2-polyethyleneimine ethoxylated/perovskite/ Spiro-OMeTAD/Au	254nm, 50 mW cm^{-2}	75days	~75%
9	ITO/SnO_2/2-(2-hydroxy-5-methylphenyl) benzotriazole-perovskite/PEAI/Spiro-OMeTAD/Au	365nm, 60 mW cm^{-2}	9h	74%

REFERENCES

1. Han, F.; Wan, Z.; Luo, J.; Xia, J.; Shu, H.; Jia, C., Planar MgxZn1-xO-based perovskite solar cell with superior ultraviolet light stability. Sol. Energy Mater Sol. Cells 2020, 208, 110417.
2. Hang, P.; Xie, J.; Li, G.; Wang, Y.; Fang, D.; Yao, Y.; Xie, D.; Cui, C.; Yan, K.; Xu, J., An interlayer with strong Pb-Cl bond delivers ultraviolet-filter-free, efficient, and photostable perovskite solar cells. iScience 2019, 21, 217-227.
3. Chen, P.; Wang, Z.; Wang, S.; Lyu, M.; Hao, M.; Ghasemi, M.; Xiao, M.; Yun, J.-H.; Bai, Y.; Wang, L., Luminescent europium-doped titania for efficiency and UV-stability enhancement of planar perovskite solar cells. Nano Energy 2020, 69, 104392.
4. Zhuang, X.; Zhou, D.; Liu, S.; Sun, R.; Shi, Z.; Liu, L.; Wang, T.; Liu, B.; Liu, D.; Song, H., Learning From Plants: Lycopene Additive Passivation toward Efficient and "Fresh" Perovskite Solar Cells with Oxygen and Ultraviolet Resistance. Adv. Energy Mater. 2022, 12 (25), 2200614.
5. Wang, M.; Yan, G.; Su, K.; Chen, W.; Brooks, K. G.; Feng, Y.; Zhang, B.; Nazeeruddin, M. K.; Zhang, Y., Ultraviolet Filtration Passivator for Stable High-Efficiency Perovskite Solar Cells. ACS Appl. Mater. Interfaces 2022, 14 (17), 19459-19468.
6. Wang, Y.; Zhang, Z.; Lan, Y.; Song, Q.; Li, M.; Song, Y., Tautomeric Molecule Acts as a "Sunscreen" for Metal Halide Perovskite Solar Cells. Angew. Chem. Int. Ed. 2021, 60 (16), 8673-8677.

7. Li, W.; Zhang, W.; Van Reenen, S.; Sutton, R. J.; Fan, J.; Haghighirad, A. A.; Johnston, M. B.; Wang, L.; Snaith, H. J., Enhanced UV-light stability of planar heterojunction perovskite solar cells with caesium bromide interface modification. Energy Environ. Sci. 2016, 9 (2), 490-498.
8. Ji, J.; Liu, X.; Jiang, H.; Duan, M.; Liu, B.; Huang, H.; Wei, D.; Li, Y.; Li, M., Two-Stage Ultraviolet Degradation of Perovskite Solar Cells Induced by the Oxygen Vacancy-Ti4+ States. iScience 2020, 23 (4).
9. Li, J.; Qi, W.; Li, Y.; Jiao, S.; Ling, H.; Wang, P.; Zhou, X.; Sohail, K.; Wang, G.; Hou, G., UV light absorbers executing synergistic effects of passivating defects and improving photostability for efficient perovskite photovoltaics. J Energy Chem. 2022, 67, 138-146.
10. Chen, P.; Wang, Z.; Wang, S.; Lyu, M.; Hao, M.; Ghasemi, M.; Xiao, M.; Yun, J.-H.; Bai, Y.; Wang, L., Luminescent europium-doped titania for efficiency and UV-stability enhancement of planar perovskite solar cells. Nano Energy 2020, 69, 104392.